REPORT DOCUMENTATION PAGE

Form Approved
OMB No. 0704-0188

1. REPORT DATE *(DD-MM-YYYY)*	2. REPORT TYPE	3. DATES COVERED *(From - To)*
02-07-2012	Conference Paper	

4. TITLE AND SUBTITLE

A Performance and Plume Comparison of Xenon and Krypton Propellant on the SPT-100

5a. CONTRACT NUMBER

5b. GRANT NUMBER

5c. PROGRAM ELEMENT NUMBER

6. AUTHOR(S)
Nakles, M.R.; Hargus Jr., W.A.; Delgado, J.J.; Corey, R.L.

5d. PROJECT NUMBER

5f. WORK UNIT NUMBER
33SP0706

7. PERFORMING ORGANIZATION NAME(S) AND ADDRESS(ES)

Air Force Research Laboratory (AFMC)
AFRL/RZSS
1 Ara Drive
Edwards AFB CA 93524-7013

8. PERFORMING ORGANIZATION REPORT NUMBER

9. SPONSORING / MONITORING AGENCY NAME(S) AND ADDRESS(ES)

Air Force Research Laboratory (AFMC)
AFRL/RQR
5 Pollux Drive
Edwards AFB CA 93524-7048

10. SPONSOR/MONITOR'S ACRONYM(S)

11. SPONSOR/MONITOR'S NUMBER(S)
AFRL-RZ-ED-TP-2012-229

12. DISTRIBUTION / AVAILABILITY STATEMENT

Approved for public release; distribution unlimited (PA #12509).

13. SUPPLEMENTARY NOTES
For presentation at the8th AIAA/ASME/SAE/ASEE Joint Propulsion Conference & Exhibit and 10th International Energy Conversion Engineering Conference, Atlanta, GA, 29 July – 2 August 2012.

14. ABSTRACT

The use of krypton as an alternative to xenon for Hall thruster propellant is an interesting option for satellite system designers due to its lower cost. However, this cost-savings comes at the expense of thrust efficiency. Reduction in efficiency can be caused by energy losses from Joule heating, radiation, and the ionization process as well as degradation of plume quality from an increase in velocity distribution spread (most often from an increase in multiply charged ion populations) and geometric beam divergence.1 In order to quantify this performance reduction for the case of the flight model SPT-100 HET (1.35 kW), performance measurements were made using an inverted pendulum thrust stand. The plume was also characterized by a Faraday probe and RPA measurements to examine how plume qualities change with operating condition. Krypton operating conditions were tested over a large range of operating powers from 800 W to 3.9 kW. Analysis of how performance is impacted by propellant and operating condition is presented. A simple mission analysis was done based on the performance measurements to evaluate the practicality of krypton propellant for an SPT-100 subsystem using krypton propellant for north-south station keeping (NSSK) for a typical communications spacecraft in geosynchronous orbit.

15. SUBJECT TERMS

16. SECURITY CLASSIFICATION OF:			17. LIMITATION OF ABSTRACT	18. NUMBER OF PAGES	19a. NAME OF RESPONSIBLE PERSON
					W.A. Hargus Jr.
a. REPORT	b. ABSTRACT	c. THIS PAGE			19b. TELEPHONE NUMBER *(include area code)*
Unclassified	**Unclassified**	**Unclassified**	SAR	24	N/A

A Performance and Plume Comparison of Xenon and Krypton Propellant on the SPT-100

Michael R. Nakles*
ERC, Inc., Edwards Air Force Base, CA, 93524
William A. Hargus, Jr.†
Air Force Research Laboratory, Edwards Air Force Base, CA 93524
Jorge J. Delgado‡ and Ronald L. Corey§
Space Systems/Loral, Palo Alto, CA 94303

The use of krypton as an alternative to xenon for Hall thruster propellant is an interesting option for satellite system designers due to its lower cost. However, this cost-savings comes at the expense of thrust efficiency. Reduction in efficiency can be caused by energy losses from Joule heating, radiation, and the ionization process as well as degradation of plume quality from an increase in velocity distribution spread (most often from an increase in multiply charged ion populations) and geometric beam divergence.[1] In order to quantify this performance reduction for the case of the flight model SPT-100 HET (1.35 kW), performance measurements were made using an inverted pendulum thrust stand. The plume was also characterized by a Faraday probe and RPA measurements to examine how plume qualities change with operating condition. Krypton operating conditions were tested over a large range of operating powers from 800 W to 3.9 kW. Analysis of how performance is impacted by propellant and operating condition is presented. A simple mission analysis was done based on the performance measurements to evaluate the practicality of krypton propellant for an SPT-100 subsystem using krypton propellant for north-south station keeping (NSSK) for a typical communications spacecraft in geosynchronous orbit.

Nomenclature

e	elementary charge
g_e	gravitational constant
I_{axial}	axial component of integrated thruster beam current
I_b	integrated thruster beam current
I_d	anode discharge current
$I_{\rm sp}$	specific impulse
j	plume charge flux
m	atomic mass
$\dot{m}_a$	anode propellant mass flow rate
$\dot{m}_i$	anode ion mass flow rate
M_0	initial spacecraft mass
M_P	propellant mass for a spacecraft
P	anode power

*Research Engineer, AFRL/RZSS, 1 Ara Rd. Edwards AFB, CA 93524
†Research Engineer, AFRL/RZSS, 1 Ara Rd. Edwards AFB, CA 93524
‡Senior R&D Engineer, Propulsion Products, 3825 Fabian Way MS G-86
§Mechanical Engineering Specialist, Propulsion Products, 3825 Fabian Way MS G-86

q	multiple for units of elementary charge
r	radial distance in thruster coordinate system
V	ion acceleration voltage
$\overline{V}$	mean ion acceleration voltage from a distribution function
V_d	anode discharge voltage
V_0	ion retarding grid potential for retarding potential analyzer
Γ	current collected by retarding potential analyzer
ΔV	average ion acceleration voltage for the thruster plume or velocity change for a spacecraft
η_a	anode efficiency
θ	angular position in thruster coordinate system or thruster cant angle
λ	plume momentum divergence half-angle, $\lambda = \arccos(< \cos(\theta) >_{mv}) \approx \arccos(< \cos(\theta) >_j)$
Φ_P	propellant utilization efficiency
Ψ_B	beam efficiency (divergence loss factor)
$<>_j$	charge flux weighted average quantity in the plume
$<>_m$	mass weighted average quantity in the plume
$<>_{mv}$	momentum weighted average quantity in the plume

Introduction

Due to a number of engineering reasons, xenon is the propellant of choice for Hall effect thrusters. These include its high mass (131 amu) and its relatively low ionization potential (12.1 eV). Furthermore, the inert nature of xenon eliminates the safety concerns that plagued early electrostatic propulsion efforts when mercury and cesium were the propellants of choice. Although xenon is a noble gas, it is the most massive, and due to its non-ideal gas behavior, it is possible to pressurize and store at specific densities that exceeded unity. As such, it can be stored at higher densities than the common liquid monopropellant hydrazine.[2]

While xenon will likely remain the ideal propellant for electrostatic electric propulsion thrusters, there are several concerns that have driven the Hall effect thruster community to explore alternative propellants. As orbit raising missions of longer duration and larger payloads are proposed for Hall effect thrusters, the mass of required propellant increases. Xenon production is a byproduct of the fractional distillation of atmospheric gases for use primarily by the steel industry. Due to the low concentration of xenon in the atmosphere (87 ppb), worldwide production appears to be limited to approximately 6,000 m^3 per year. Increasing industrial demand for items such as high efficiency lighting and windows has produced wide price swings in the past decade. Xenon prices have varied by as much as a factor of ten.

For high thrust to power missions, bismuth has been demonstrated as a viable alternative Hall effect thruster propellant. Bismuth, with its high atomic mass (209 amu) and low ionization potential (7.3 eV) appears to have advantages for missions where high thrust at reduced specific impulse is advantageous, such as orbit raising missions. Bismuth's main drawback is that the metal must be vaporized to be ionized and accelerated within a Hall effect thruster. The requirement for high temperatures (boiling point of 1,837 K) require special engineering considerations compared to the relatively simple gas distribution systems used for xenon. In addition, the use of vapor as a propellant has tended to cause concern for spacecraft operators despite the assurances of thruster developers. The risk of metal redeposition from the propellant on solar arrays and sensitive instruments is a large concern that will strongly limit bismuth's appeal to spacecraft designers.

For missions that can benefit from higher specific impulse, krypton may have some benefits. Krypton has a lower atomic mass (83.8 amu) and a higher ionization potential (14.0 eV) than xenon. However like xenon, krypton is a noble gas and could be easily integrated into existing xenon propellant management systems without much modification. The small difference in ionization potential is unlikely to dramatically affect the efficiency of a Hall effect thruster, and the lower mass would produce a 25% increase in specific impulse assuming there were no offsetting losses. The increase in specific impulse would be useful for missions such as GEO communications satellite north-south station keeping. For missions such as orbit raising, increasing the specific impulse will increase trip time due to power limitations. However as solar electric power system specific power decreases, increasing the specific impulse of the propulsion system is advantageous.

Krypton is approximately 10 times more common in the atmosphere (and hence in production) than xenon, and when accounting for mass is approximately 6 times less expensive. One disadvantage for krypton

is that its tankage fraction appears to be substantially higher than that of xenon due to reduced van der Waals interactions. As such, compressed gas tankage fractions could be as high as 37%. At least one study has examined this issue and has identified space rated cryo-coolers that could liquefy krypton (120 K boiling point), or for that matter xenon (165 K boiling point), and reduce tankage fractions to less than 2%.[2]

Experimental studies have often shown thrust efficiency with krypton propellant to be inferior to that of xenon.[3,4,5] However, for a 50 kW HET similar thrust efficiency was attained with krypton propellant.[6] Russian studies[4,7,8] have investigated using a mixture of krypton and xenon propellant for SPT thrusters to achieve a performance compromise at a cost cheaper than either pure xenon or pure krypton. This mixture of xenon and krypton is a byproduct of liquid oxygen manufacturing and costs 15 times less than pure xenon and 2-3 times less than pure krypton.[7] Its use has shown promising results on the SPT-100 and SPT-140 thrusters.

The goal of this ongoing study is to characterize the differences between xenon and krypton performance and plume characteristics for a Hall effect thruster with extensive flight heritage. The SPT-100 thruster was chosen for this study because it is among the most well-established Hall effect thrusters in the space propulsion industry. SPT design heritage dates back to the 1960s and 70s in the former U.S.S.R. After the break up of the Soviet Union, the Ballistic Missile Defense Organization (BMDO) lead efforts to transfer SPT technology to the United States so that western spacecraft could benefit from their attractive combination of thrust and efficiency.[9] The SPT-100 thruster, designed and built by Fakel, was extensively tested for lifetime[9] and performance[9,10] by NASA in the early 1990's. In 1991, Space Systems/Loral (SS/L) partnered with Fakel to flight qualify the SPT-100 and a corresponding power processing unit (PPU) for U.S. flight standards. To date, SS/L has launched seven spacecraft with SPT-100 propulsion subsystems and has eleven more spacecraft under construction. This SPT subsystem now has more than thirteen years of cumulative on-orbit experience with a single thruster accumulating over 6 years of near-daily operation.[11]

This paper will present the results from thruster performance testing and probe measurements. Although the design of the SPT-100 is optimized for xenon, this exploratory investigation should provide some insight into the possibilities of using krypton as a propellant in Hall effect thrusters, primarily due to its low cost and possible application as a low-development overhead replacement for existing xenon Hall effect thruster systems.

Experimental Apparatus and Techniques

Test Facility

The tests performed in this study utilized Chamber 1 at the Air Force Research Laboratory at Edwards Air Force Base. Chamber 1 is a cylindrical non-magnetic stainless steel vacuum chamber 2.4 m in diameter and 4.1 m in length. Pumping is provided by two liquid nitrogen baffled (70 K), 1.2 m flanged gaseous helium two stage cryogenic (15 K) vacuum pumps. Chamber pressure is monitored with a cold cathode gauge. Background pressure for nominal thruster operation was measured to be 1.1×10^{-5} Torr for xenon (at 56.4 sccm propellant flow rate) and 1.0×10^{-5} Torr for krypton (at 65.4 sccm propellant flow rate) with gas correction factors applied.

For probe testing, the thruster is mounted atop a cantilevered beam and aligned with a probe translation system. The translation system (Fig. 1(c))combines a rotary stage and a linear translational stage to enable sweeping of various plasma interrogation probes in the $r - \theta$ plane. The rotary stage is capable of rotating between $\pm 90^{\circ}$ from the plume axis and the linear translation stage allows probe traversing up to 100 cm from the thruster exit plane.

Hall Effect Thruster

A flight model SPT-100 Hall effect thruster was used in this study. The thruster is equipped with two lanthanum hexaboride (LaB_6) cathodes (only one was used during these tests). Photographs of the thruster are shown in Fig. 2. This thruster has a conventional five magnetic core (one inner, four outer) magnetic circuit. Discharge current is routed through the magnetic circuit and thus no extra power source for the magnets is required. The acceleration channel of the thruster has a 100 mm outer diameter, a 50 mm inner diameter. The thruster has been characterized to have a thrust of 83 mN with a specific impulse of 1,600 s, yielding an anode efficiency near 50%.[9] The thruster and cathode were powered with commercial off-the-shelf Sorenson power supplies instead of the PPU used on-orbit. A computer data acquisition system recorded

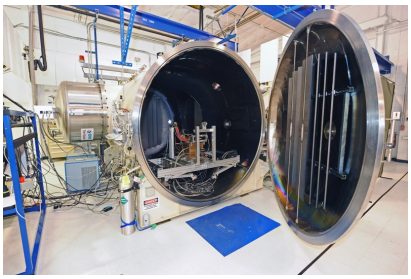

(a) Chamber 1 test facility.

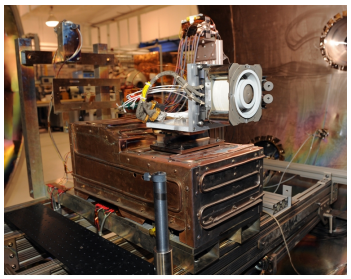

(b) The null-type inverted pendulum thrust stand used for performance measurements.

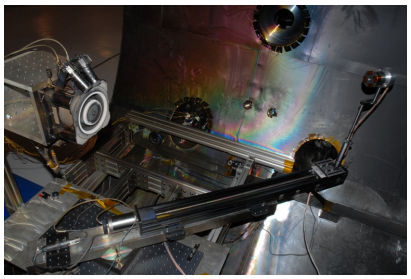

(c) Probe translation system used for RPA and Faraday probe measurements.

Figure 1. Hall thruster testing facilities at the Air Force Research Laboratory at Edwards Air Force Base.

the potential and current outputs of the power supplies used in the thruster operation at a rate of 2 Hz during this study. For propellant flow, digital mass flow controllers from Aera dispersed gas to the anode and cathode taking the place of the xenon flow control system (XFC) used on-orbit.

Thrust Stand

The thrust stand used in these performance measurements was of the widely-used null-type, inverted pendulum design by Haag[12] at NASA Glenn Research Center. As force is applied to the inverted pendulum, translation is counteracted by an electromagnetic force generated by a feedback system using a PID controller. Displacement of the pendulum relative to a mirror is detected optically with a linear displacement gap transducer (LDGT) with a fiber optic sensor. When displacement is detected from a given zero point, current is flowed through a null coil to generate a restoring force applied to a concentrically mounted magnetic rod connected to the pendulum. This restoring force is linearly proportional to the voltage applied to null coil. A calibration curve correlating null coil voltage to restoring force is generated mechanically by loading and unloading weights of known value to the pendulum with a pulley system. The constant of the linear calibration curve is sensitive to the thermal changes of thrust stand and therefore thrust measurement values tend to drift as an operating thruster dissipates heat to the thrust stand. To prevent large temperature swings, chilled ethylene glycol was flowed through tubing on the thrust stand's copper shroud.

Probes

Faraday Probe

Ion current flux was measured using a guarded Faraday probe pictured in Fig. 3(a). The electrodes were constructed from molybdenum. Ion current was collected with a disk measuring 8.3 mm in diameter. A concentric guard piece, measuring 22.5 mm in outer diameter, was used to minimize the effects of the plasma sheath on the ion current collector's effective collecting area. A 0.56 mm wide gap existed between the outer wall of the collector and the inner wall of the guard ring. The effective current collector area of the probe was calculated by adding a portion of the gap surface area to the collector surface area. The amount of gap area considered to contribute to the effective current collector area was proportional to the ratio of lateral wall surface area of the collector to the total lateral wall surface area on both sides of the gap as suggested in Ref. 13. Ion charge flux was measured by dividing the current to the collector by its effective surface area. The disk and guard ring were biased to -30 V with respect to chamber ground during the measurements so that ion saturation was achieved. The effects of secondary electron emission were assumed to be less than a few percent[14] and were neglected in the analysis of the measurements.

Retarding Potential Analyzer

The retarding potential analyzer (RPA) used in this experimental investigation was a four grid design described in detail in Ref. 13. The RPA operates as an energy filtered Faraday probe. The energy filtering is accomplished using a series of biased grids in front of the current collector.

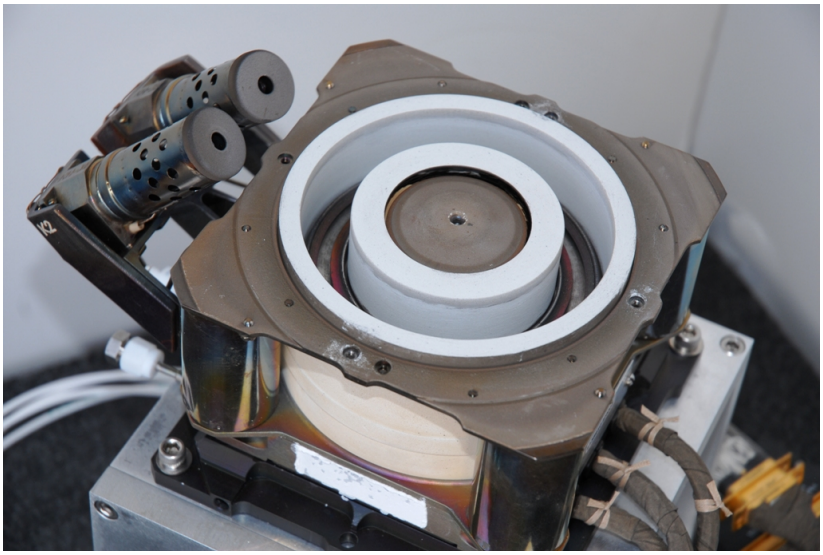

(a) SPT-100 flight model.

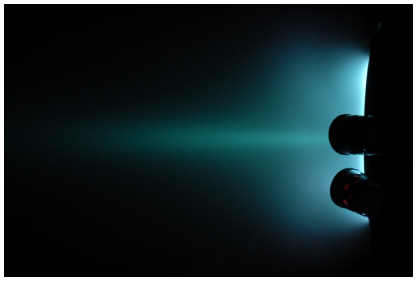

(b) Thruster operating on xenon propellant.

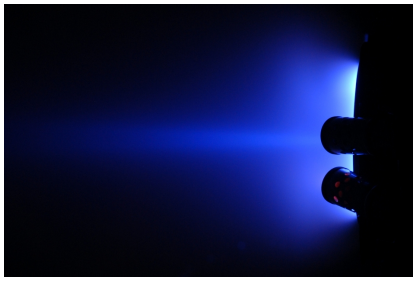

(c) Thruster operating on krypton propellant.

Figure 2. Photographs of the SPT-100 thruster used in this study.

The first grid acts as an aperture to reduce plasma flow into the probe and is allowed to float at the local plasma floating potential. The second grid (electron repulsion), biased negatively with respect to chamber ground, repels incoming electrons within the plasma while allowing ions to pass through. The potential of the ion retarding grid (third grid) is swept positively relative to chamber ground to allow selective passage of ions based on their kinetic energy. The fourth grid (electron suppression) is placed in front of the collector to suppress ion impact induced secondary electron emission.

Current to the collector is measured as a function of ion retarding grid potential. The probe current is differentiated with respect to ion retarding potential to calculate an energy-per-charge distribution function. Analytically, for a single species, the derivative of the current per unit area is[15]

$$\frac{\mathrm{d}\Gamma}{\mathrm{d}V_0} = \frac{qe}{m} f(V) \tag{1}$$

which is proportional to the ion energy-per-charge distribution of the plasma.

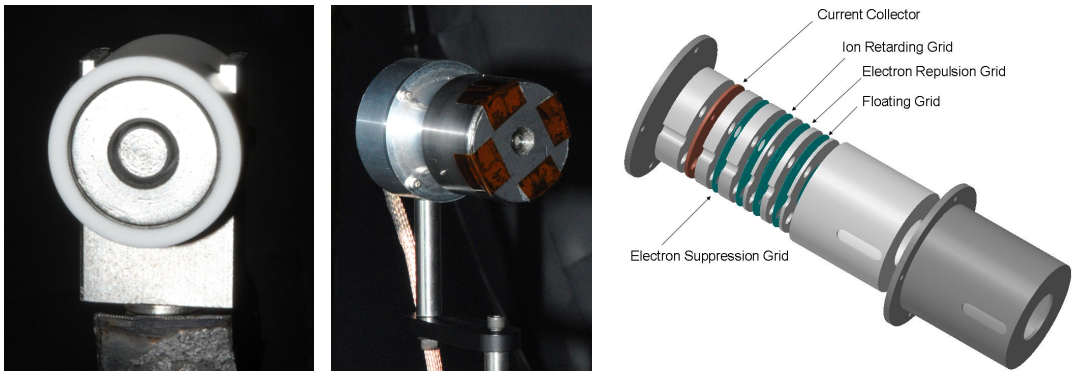

(a) Photograph of Faraday Probe. (b) Photograph of RPA. (c) Exploded view of the RPA showing grid placement.

Figure 3. Faraday probe and retarding potential analyzer (RPA) used for plume analysis.

Testing Matrix and Methodology

Testing Matrix

The goal of this study was to test the performance of the SPT-100 operating on krypton gas over a large range of thruster power conditions through variations in both discharge potential and propellant flow rate and to test a smaller set of xenon cases for comparison. The krypton testing matrix for this study emphasized higher than nominal power (1.35 kW) cases. Studies of krypton propellant have documented that increased flow rate will improve the propellant utilization fraction.[16] A lower propellant utilization fraction is one of the major reasons krypton performance has been known to be inferior to that of xenon. A promising feature of krypton is that it can potentially have a higher specific impulse than xenon due to its lower atomic mass. Therefore, exploration of operating conditions at higher than nominal discharge potential was of interest (specific impulse is proportional to the square root of discharge voltage) to see if advantageous specific impulse could be realized in spite of krypton's inferior propellant utilization. It should be noted that for lower than nominal power krypton cases, anode ignition was more difficult and sometimes required ignition at nominal discharge voltage before dropping the discharge voltage to a lower value. Besides the expected low performance at low power, this ignition difficulty may render lower than nominal power conditions impractical for implementation on a flight PPU.

Exploratory runs of the thruster were conducted with both propellants to ascertain the mass flow rate value that produced the nominal 4.5 A discharge current for thruster operation. In order to mimic the XFC used for the on-orbit PPU subsystem, a 13:1 propellant split was maintained between the anode and the cathode for all operating conditions so that cathode flow rate accounted for approximately 7% of the total propellant usage. (In this study, performance parameters are calculated using the combined anode and cathode mass flow rates.) The nominal flow rates for this study were 5.54 mg/s for xenon and 4.09 mg/s for krypton. Off-nominal flow rate conditions were set relative to these values in the testing matrix.

It was noted that the nominal xenon flow rate for this study was a little higher than reported in other studies.[9,10] This discrepancy may be due to variation in calibration between the XFC used in these studies and the digital mass flow controllers used here. The mass flow controllers in this study were calibrated with a molbloc system from DH Instruments using xenon gas. The molbloc system measures pressure and temperature differences in laminar flow across a calibrated flow element to determine flow rate. These xenon calibrations for the mass flow controllers were assumed to also apply to krypton due to the fact the manufacturer's calibration conversion factors from the surrogate gas of argon to the actual operating gas are the same for xenon and krypton (due their similar thermal properties).

For the krypton performance testing matrix, a total of 7 mass flow rates and 12 discharge current potentials were tested. Mass flow rates ranged from -20% to +40% of the nominal vaule. For discharge potential, values between -20% to +90% of nominal were tested. Parameters were varied in increments of 10% of their nominal values as ilustrated in Table 1. For xenon performance testing, mass flow rates and discharge potentials ranging from -30% to +30% relative to their nominal values were also tested in increments of 10% of their nominal value. However for xenon, combinations of off-nominal flow rates and off-nominal discharge voltages were not tested.

After performance characterization was complete, electrostatic probe measurements were made at a later date for all of the xenon operating conditions and a subset of the krypton operating conditions. See Tables 1 and 2 for details.

It should be noted that no magnetic field optimization was performed for any operating condition on this flight model thruster. The magnet current was purely determined by the operating condition discharge current. No additional current was added to the magnetic circuit via an extra power supply.

Table 1. Krypton operating condition test matrix. Table values are operating condition power (W). "F" and "R" denotes Faraday probe and RPA measurements were taken, respectively.

Flow Rate ⇒	-20%	-10%	**Nominal**	+10%	+20%	+30%	+40%
Dis. Potential ⇓	(3.27 mg/s)	(3.68 mg/s)	**(4.09 mg/s)**	(4.50 mg/s)	(4.90 mg/s)	(5.31 mg/s)	(5.72 mg/s)
-20% (242 V)	813	950	1083 (F, R)	1209	1339 (F, R)	1476	1606 (F, R)
-10% (272 V)	915	1069	1220	1363	1511	1671	1820
Nom. (302 V)	1015	1187	**1356** (F, R)	1516	1681 (F, R)	1863	2033 (F, R)
+10% (332 V)	1121	1306	1491	1670	1852	2054	2258
+20% (363 V)	1242	1431	1628 (F, R)	1823	2023 (F, R)	2248	2468 (F, R)
+30% (393 V)	1356	1561	1769	1977	2208	2445	2675
+40% (423 V)	1468	1693	1913 (F, R)	2143	2376 (F, R)	2615	2878 (F, R)
+50% (453 V)	1567	1821	2061	2302	2547	2799	3078
+60% (483 V)	1662	1938	2213 (F, R)	2463	2720 (F, R)	2987	3276 (F, R)
+70% (513 V)	1751	2048	2347	2624	2895	3195	3481
+80% (544 V)	1857	2171	2480 (F, R)	2765	3063	3389	3690
+90% (574 V)	1960	2289	2605	2929	3245	3589	3913

Table 2. Xenon operating conditions tested. Table values are operating condition power (W). Faraday and RPA measurements were made for every test case. Note: Blank values represent untested conditions.

Flow Rate ⇒	-30%	-20%	-10%	**Nominal**	+10%	+20%	+30%
Dis. Potential ⇓	(3.88 mg/s)	(4.44 mg/s)	(4.99 mg/s)	**(5.54 mg/s)**	(6.10 mg/s)	(6.65 mg/s)	(7.21 mg/s)
-30% (211 V)				945			
-20% (242 V)				1077			
-10% (272 V)				1213			
Nom. (302 V)	916	1061	1207	**1351**	1508	1666	1829
+10% (332 V)				1493			
+20% (363 V)				1638			
+30% (393 V)				1785			

Thrust Stand Testing Methodology

Before and after each series of thrust measurements, an in situ calibration of the thrust stand was performed using its mechanical weight loading system to produce a calibration curve. After the initial thrust stand calibration, the thruster was turned on at its nominal operating condition. As the thruster warmed up, its anode current would rise during the first minute of operation and then gradually fall to the nominal 4.50 A value over the course of about half an hour. When the discharge current stabilized at its nominal value, the thruster was considered to be warmed up. For off-nominal flow rate tests, an extra warm up period was given where the propellant flow rate was adjusted to its new value and then the thruster was run until its discharge current stabilized (typically 15 minutes or less).

After thruster warm up was complete, an updated linear thrust stand calibration constant was determined by turning off the anode discharge (both voltage and mass flow) for about 1 minute so that the null coil voltage could be recorded. The cathode discharge was maintained during this period by applying potential to the igniter. The anode discharge was then reignited with the desired operating conditions for testing. The operating condition for testing was run for 15 minutes. Then the anode discharge was turned off again to find the new calibration constant. This process was repeated for a series of measurements. The slope of the calibration curve was found to be stable to three digits of precision even after several hours thruster operation. For operating conditions in the krypton test matrix, conditions with the same mass flow rate were typically tested consecutively.

During post test data analysis, the thermal drift rate of the calibration constant for each test condition was linearly approximated using its values before and after the test and the time between its measurements. Thrust data was sampled from the end of the testing time period for a duration where the thermal drift was estimated to be no more than 0.1 mN in most cases. However, sampling duration was constrained to be between 1 and 5 minutes.

Probe Derived Plume Efficiency Analysis

Probe measurements were used to study the individual components of anode efficiency to determine how plume characteristics affect performance for the various operating conditions. Reference 1 outlines a standard analytical methodology for Hall thruster efficiency analysis. Anode efficiency is separated into the product of energy efficiency, beam efficiency, and propellant utilization efficiency. The anode efficiency can be expressed as

$$\eta_{\mathrm{a}} = \left(\frac{\Delta V}{V_d}\right)\left(\frac{I_b}{I_d}\right)\Phi_{\mathrm{P}}\Psi_{\mathrm{B}} \tag{2}$$

where the first two terms comprise the energy efficiency. Energy efficiency accounts for losses due to Joule heating, radiation, and ionization processes. It is completely separated from jet vector properties. The third term, propellant utilization efficiency, accounts for losses associated with dispersion of the jet VDF due to incomplete ionization and the presence of multiple ion species with widely varying velocities. The last term, beam efficiency, quantifies losses due to geometric plume divergence.

Faraday probe measurements can be used to approximate both the current utilization efficiency and the beam efficiency. The beam current can be calculated as

$$I_b \approx \pi r^2 \int_{-\frac{\pi}{2}}^{\frac{\pi}{2}} j(\theta)\,|\sin\theta|\mathrm{d}\theta \tag{3}$$

The ratio of beam current to the anode current (recorded by the data acquisition system) is the current utilization efficiency.

Beam efficiency is a measure of jet momentum loss due to beam divergence. It is defined as the ratio of axial momentum that produces thrust to the total momentum exhausted in the plume. It can be approximated using charge flux weighted average divergence

$$\Psi_{\mathrm{B}} = <\cos\theta>_{mv}^{2} \approx \left(\frac{I_{\mathrm{axial}}}{I_b}\right)^2 \approx \left(\frac{\pi r^2 \int_{-\frac{\pi}{2}}^{\frac{\pi}{2}} j(\theta)\cos\theta\,|\sin\theta|\mathrm{d}\theta}{\pi r^2 \int_{-\frac{\pi}{2}}^{\frac{\pi}{2}} j(\theta)\,|\sin\theta|\mathrm{d}\theta}\right)^2 \tag{4}$$

Voltage utilization efficiency is the ratio of average ion acceleration voltage to anode discharge voltage. Being a part of the energy efficiency, it contains no dependency on vector properties of the jet. Voltage utilization can be calculated as

$$\left(\frac{\Delta V}{V_d}\right) = \left(\frac{<\overline{V}(\theta)>_m}{V_d}\right) \approx \frac{1}{V_d}\left(\frac{\pi r^2 \int_{-\frac{\pi}{2}}^{\frac{\pi}{2}} j(\theta)\overline{V}(\theta)\,|\sin\theta|\mathrm{d}\theta}{\pi r^2 \int_{-\frac{\pi}{2}}^{\frac{\pi}{2}} j(\theta)\,|\sin\theta|\mathrm{d}\theta}\right) \tag{5}$$

where a charge flux weighted approximation enables calculation through a combination of RPA and Faraday probe data.

Due to the charge flux weighted approximations and uncertainty in the probe measurements (especially due to low energy ions) there is a potentially large error associated with anode efficiency subcomponents derived from probe measurements. However, good precision was observed in the calculated efficiencies making them useful for observing trends and relative comparison between different test cases.

Results and Discussion

Performance Data

The results of the performance measurements are presented in Figs. 5 and 6. Figure 5(b) shows that anode current was very stable (less than 2% variation) at any given mass flow rate condition throughout the range of discharge potential tested. Thrust measurements were found to be very repeatable throughout most of the testing (to within better than ±0.5 mN in most cases). However, a small data continuity issue arose toward the end of the krypton matrix testing. Thrust measurement values became slightly higher compared to data points taken earlier by about 2% and thus appeared slightly discontinous compared to the exisiting performance data. Unfortunately, the reason for this discrepancy was never determined. Performance variation was seen in other reported tests.[9] Measurements affected by this issue were at the +30% propellant flow rate condition (discharge potentials: 390, 510-570 V) and the +40% propellant flow rate conditions (discharge potentials: 330-570 V). Despite this minor discrepancy issue, the trends of the krypton performance data are still apparent.

Thrust values are plotted as a function of discharge potential in fig. 5(c) and thruster power in fig. 5(d). At the nominal operating condition, the thrust value for krypton (62.9 mN) was lower than that of xenon (82.1 mN) by 23%. Thrust was seen to increase in an approximately linear manner with increasing discharge voltage. In the case of krypton, there was a noticable point of diminished gains around 510 or 540 V. Thrust also increased in a linear manner for increasing propellant flow rate throughout the range of flow rates test.

Specific impulse data for the tested cases are presented in Figs. 5(e), 5(f), and 6(b). One of the main physical reasons that krypton is an interesting alternative propellant choice for low-thrust missions is for its potentially greater specific impulse due it its lower atomic mass relative to xenon. However, this potential gain in specific impulse was not realized in the case of the SPT-100 flight model thruster. At nominal conditions, krypton specific impulse was measured at 1568 s, which was virtually no improvement over the 1511 s measured for xenon. The ideal anode specific impulse for a given anode voltage can be calculated as

$$I_{\mathrm{sp}} = \frac{1}{g_e}\sqrt{2\frac{q}{m}V_a} \tag{6}$$

when all of the propellant is assumed to be completely converted into singly charged ions that are accelerated through the entire anode potential in a perfectly collimated beam. Ideally, krypton would have a 25% greater specific impulse than xenon. Figure 6(b) shows a comparison of the measured anode specific impulse to the ideal value. (Note that the anode specific impulse calculation uses only the anode mass flow rate instead of the total flow rate.) Nominal flow rate krypton cases were found to have an almost constant 1000 s gap between their actual anode specific impulse and the ideal value across the range of tested anode potential. This translated into a 37% deficiency at the nominal 302 V condition. Xenon propellant cases were found to have an approximately 520 s difference between their actual value and their ideal values. The performance gap at 302 V was 24% for xenon. The reason for the lower realization of ideal specific impulse for krypton compared to xenon was likely its inferior propellant utilization fraction ($\dot{m}_i/\dot{m}_a$). Non-ionized propellant decreases the bulk velocity of the plume and thus lowers specific impulse. Due to the faster neutral velocity and lower ionization cross section of krypton, a higher specific mass flow rate ($\dot{m}_a$/m) is needed for effective

propellant ionization than for xenon for a given channel length and cross section.[17] However, only small improvements were made in specific impulse for krypton as mass flow was increased above the nominal value. Faraday probe data in this study also suggest that beam divergence losses also account for some of the unrealized specific impulse gain.

Thrust efficiency (calculated with the combined anode and cathode flow rate) is plotted in Figs. 6(c) and 6(d). For the nominal operating condition, the efficiency value was 44% for xenon and 36% for krypton. For krypton, efficiency was observed to rise with anode potential until a peak value around 510 to 540 V and then decrease at the highest potentials. To acheive a similar efficiency for krypton, higher thruster operating power is required. For the nominal flow rate, an anode potential of 453 V would be necessary, resulting in a 700 W operating power increase. Increasing propellant flow rate improved efficiency, most noticeably for low flow rate conditions, which can be explained by better propellant ionization.

In studies of a laboratory model SPT-100 operating on krypton by Kim,[4] current to the magnetic coils was adjusted to minimize anode current. Anode efficiency data were presented at an anode flow rate of 5 mg/s, which was a similar flow rate to the +30% flow rate setting of the present study where anode flow rate was 4.93 mg/s. Comparison of the present study (Fig. 6(e)) to Kim's data enabled the effects of magnetic field optimization to be observed. In Kim's data, anode efficiency was about 4% greater for anode potentials less than 400 V. However, anode efficiency for both data sets matched well for anode potentials of 400 V and higher, which may indicate the presence of an ideal magnetic field for these high anode potential conditons for the flight model SPT-100. Kim also tested a thruster configuration that used an additional magnetic coil to dramatically change the magnetic field topography of the thruster. This alteration was seen to signficantly improve anode efficiency for krypton. For one operating condition, the anode efficiency of krypton was improved by about 6%. Surprisingly, there was signficant disagreement in anode efficiency data for xenon between these two studies. The lack of magnetic field optimization may be why values in the present study were lower.

Probe Data

Faraday Probe

Faraday probe sweeps were taken in radial increments of 5 cm from $r = 50$ cm to $r = 100$ cm. The angular range of the sweeps was from θ = -90° to $\theta = 90°$. Measurements were taken with a 1° angular resolution for krypton cases and 2.5° resolution for xenon cases. The Faraday probe measurements are shown in Figs. 7 and 8.

Beam current per solid angle was observed to have a dependency on radius likely due to collisions in the plume from the chamber background pressure. This led to a defocusing of the beam where charge flux decreased in the plume core and increased at oblique angles as measurement radius increased. Figure 8(e) shows the evolution of the plume charge flux as a function of radius for a nominal condition xenon case. To account for the effect of collisions, charge flux was linearly interpolated as a function of radius to approximate its value at the exit plane ($r = 0$). This corrected charge flux was used in the calculation of integrated beam current and beam efficiency.

For both propellants, the distribution of charge flux was observed to be strongly dependent on discharge potential where increases in discharge potential led to a higher degree of beam focusing (Figs. 7(a), 7(b), 7(e), 7(f)). Mass flow variations led to a proportional change in charge flux magnitude where the general shape of the distribution remained nearly the same (Figs. 7(c), 7(d), 8(a), 8(b)).

The krypton plume was generally more divergent than the xenon plume as seen in Fig. 8(c). At nominal power, the 90% beam current half-angle was 7° greater for krypton. As a result, the krypton plume beam efficinency was approximately 0.08 lower than that of xenon for a given discharge potential.

Current utilization efficiency was similar for both the nominal condition xenon and krypton plumes as seen in Fig. 12(d). Increases in propellant flow rate and discharge potential were observed to create small improvements for krypton, but not for xenon.

Inferior propellant utilization fraction is typically a major reason for krypton's lower performance in electric propulsion devices. Due to the fact that ion charge species fractions were not determined in these experiments, propellant utilization fraction could not be calculated directly. However, its product with average ion charge, Q, was plotted in Fig. 12(e) to observe its general behavior. The plot suggests that propellant utilization fraction improves significantly for krypton as propellant flow rate is increased. For xenon the improvements appear to be much smaller.

RPA

Retarding potential analyzer data was taken at a radius of 100 cm from the thruster exit plane from θ = -90° to θ = 90° in 5° increments. Plasma potential was not measured in these experiments and thus the difference between plasma potential and ground potential (assumed to be less than a few percent of the discharge voltage) was neglected in this RPA analysis. The RPA data are shown in Figs. 9 and 10.

An EDF comparison for the xenon and krypton nominal condition is given in Fig. 11. It shows that the most probable energy is consistently 6 V less for krypton. The EDF distribution shape is similar for both propellants for the primary beam ions. However, at high angles, the xenon data exhibited a low energy peak significantly higher than that of krypton.

The mean of the EDF as a function of θ (Figs. 9(e), 9(f), 10(e), and 10(f)) was used in Eqn. 5 to predict the voltage utilization efficiency. The results are shown in Fig. 13(d). However, due to instrument uncertainty in the low energy portions of EDF traces from RPA's, the most probable EDF value is often used for the mean in the calculation of voltage utilization efficiency. Voltage utilization calculated with this technique is shown in Fig. 13(f). A third method for estimating voltage utilization efficiency was also explored. In this method the mean EDF value was calculated by only integrating the portion of the curve above 100 eV/q and thus avoiding the low energy peak. The results of this method are shown in Fig. 13(e).

The results of the 1st and 3rd methods produced voltage utilization efficiency estimates with similar trends, but with a constant offset in magnitude of about 0.03. For these methods, voltage utilization efficiency increases with discharge potential to a certain point and then decreases. For the most probable EDF value method, the voltage utilization efficiency increases with discharge potential for all values tested. All methods show that voltage utilization is better for xenon that krypton.

Krypton Mission Example

A simplified example mission was studied to evaluate the possibility of using krypton propellant for the flight model SPT-100 on a spacecraft based on the performance measurements in this study. This example mission was intended to replicate the general requirements of a propulsion system for north-south station keeping on a communications satellite in geosynchronous orbit. In this example, the spacecraft would have the following characteristics and requirements:

- Initial spacecraft mass: 3760 kg
- Mission lifetime: 15 years
- Thruster cant angle: 40 ° (directional cosine loss)
- Quantity of SPT-100 thrusters: 2
- Delta-V required: (51 m/s/year)×15 years = 765 m/s

The propellant mass required for this mission can be calculated from the basic rocket equation as:

$$M_p = M_0 - M_0 \exp\left(\frac{-\Delta V}{g_e I_{\mathrm{sp}} \cos\theta}\right) \tag{7}$$

The resulting propellant mass for the mission is divided between the two thrusters. The number of required operational hours for each thruster is determined by dividing the propellant mass for each thruster by the propellant flow rate for its operating condition. The results of this analysis are plotted in Fig. 4.

In Fig. 4. propellant mass per thruster is plotted versus the required operational time per thruster for the matrix of krypton operating conditions tested. Operating condition data points fall along lines of propellant flow rate. Linear interpolation was used to create contours for the operational power required per thruster for krypton propellant. As propellant mass and operational time requirements decrease, the power requirement increases. The tested xenon operating conditions are also displayed for reference.

A mission using xenon at the nominal operating condition (1356 W) would require 6.1 years of operational time per thruster and 120 kg of propellant per thruster. This condition is marked for reference on the plot. The data for xenon operating with the nominal discharge potential as propellant flow rate varies is marked with a red line. This forms a boundary for operating conditions that would have a propellant mass savings relative to xenon operating at its nominal discharge voltage. Tests have validated the SPT-100 life time

as exceeding 2.71 million N-s (equivalent to approximately 9000 hours of operational time) for xenon at the nominal condition.[18,11] This boundary is also marked in red for reference. Some krypton operating conditions within these boundaries may be feasible for completing this mission. Although it should be noted that most of these krypton cases require a significantly higher power throughput than the life tested nominal xenon condition and thus may limit the lifetime of the thruster to values lower than the validated xenon figure. Thruster erosion rates with krypton are unknown so life testing would be required to determine reasonable operational times.

One krypton operating condition that may be appropriate is the 390 V, nominal flow rate setting. Using this setting, 54 kg of total propellant mass could be saved relative to the nominal xenon operating condition. However, 400 W of extra power per thruster and an extra 400 hours of firing time for each thruster would be required. It should be noted that off-nominal condition xenon cases could be chosen for fuel savings and they would offer better overall performance than the krypton operating conditions studied. As seen in the performance data, the krypton operating conditions did not offer significantly better specific impulse than xenon so choosing krypton propellant for potential mass savings may not be a good idea. Also, krypton propellant has a higher tankage fraction and may require larger or more massive tanks for storage. The potential benefit krypton propellant could offer would be its cheaper price.

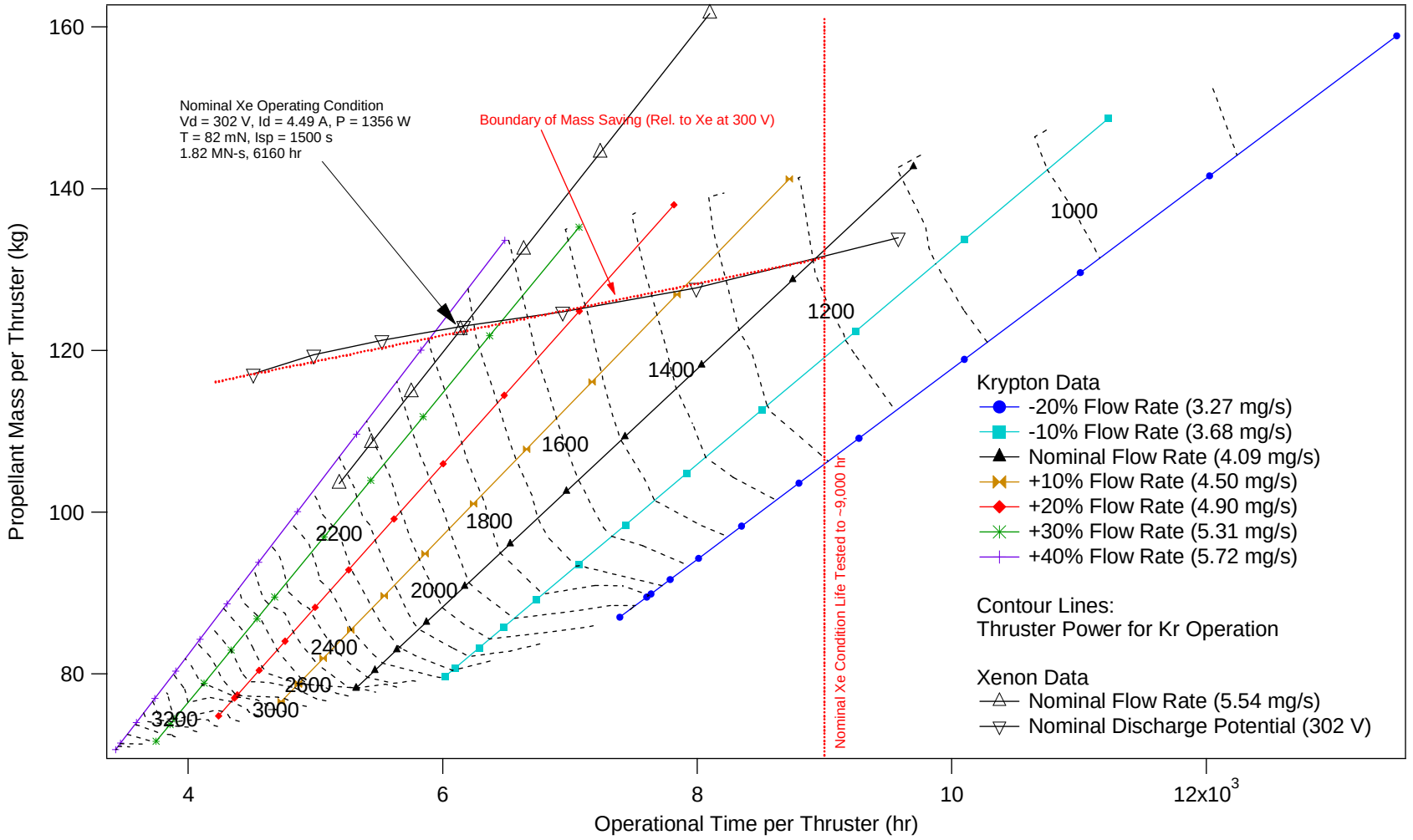

Figure 4. Simplified mission analysis for an SPT-100 propulsion subsystem with two thrusters operating on krypton propellant for north-south station keeping. In this example, the spacecraft has an initial mass of 3760 kg and a lifetime delta-V requirement of 765 m/s.

Conclusions

A large range of krypton operating conditions spanning a power range of 800 W to 3.9 kW were tested for performance for the flight model SPT-100. Thruster performance was significantly lower compared to operation on xenon propellant. Specific impulse for krypton operation was not substantially higher than that of xenon, which does not make krypton a practical choice for propellant mass savings. The disparity of krypton's performance is largely due to its lower propellant utilization fraction, which is not surprising because the acceleration channel geometry design was optimized for xenon. Faraday probe measurements suggest that inferior beam efficiency may also be a significant reason for the decreased performance. Thruster efficiency on krypton was about 8% lower than for xenon at the nominal operating condition, but it is possible to increase krypton thruster efficiency to levels around 50% using higher power operating conditions. However, the higher operating power required to improve the performance may lead to a shorter life time. If krypton is to be seriously considered for on-orbit use, erosion studies and life testing would be required to validate the thruster's ability to meet mission duration specifications. If xenon prices increase dramatically in the future, krypton may still be a feasible fuel alternative for the SPT-100. Despite reduced performance, krypton still may be able to fufill station keeping requirements for certain missions. The thruster performance also has the potential to be improved for krypton though design modificatons as Kim[4] has demonstrated using an altered magnetic field configuration for the SPT-100 laboratory model.

Acknowledgments

The authors would like to thank Paul Adkison, Joseph Blakely, and Garrett Reed from AFRL for their assistance with the thrust stand setup and instrumentation programming. They would also like to thank Robert Lobbia and Dan Brown from AFRL for helpful discussions on probe data analysis.

References

[1]Brown, D. L., Larson, C. W., and Beal, B. E., "Methodology and Historical Perspective of a Hall Thruster Efficiency Analysis," *Journal of Propulsion and Power*, Vol. 25, No. 6, 2009, pp. 1163–1177.

[2]Duchemin, O., Valentian, D., and Cornu, N., "Cryostorage of Propellants for Electric Propulsion," *45th AIAA/ASME/SAE/ASEE Joint Propulsion Conference, No. AIAA-2009-4912*, Denver, CO, 2009.

[3]Linnell, J. A. and Gallimore, A. D., "Efficiency Analysis of a Hall Thruster Operating with Krypton and Xenon," *Journal of Propulsion and Power*, Vol. 22, No. 6, November-December 2006, pp. 1402–1412.

[4]Kim, V., Popov, G., Kozlov, V., Skrylnikov, A., and Grdlichko, D., "Investigation of SPT Performance and Particularities of its Operation with Kr and Kr/Xe Mixtures," *In the Proceedings of the 27th Electric Propulsion Conference*, No. IEPC-01-065, 2001.

[5]Marrese, C., Haas, J. M., Domonkos, M. T., Gallimore, A. D., Tverdokhlebov, S., and Garner, C. E., "The D-100 performance and plume characterization on krypton," *Proceedings of the 32nd AIAA/ASME/SAE/ASEE Joint Propulsion Conference and Exhibit*, No. AIAA 96-2969, 1996.

[6]Jacobson, D. T. and Manzella, D. H., "50 kW Class Krypton Hall Thruster Performance," *In the Proceedings of the 39th AIAA/ASME/SAE/ASEE Joint Propulsion Conference*, No. AIAA 2003-4550, 2003.

[7]Arkhipov, B., Koryakin, A., Murashko, V., Nesterenko, A., Khoromsky, I., Kim, V., Kozlov, V., Popov, G., and Skrylnikov, A., "The Results of Testing and Effectiveness of Kr-Xe Mixture Application in SPT," *In the Proceedings of the 27th International Electric Propulsion Conference*, No. IEPC-01-064, 2001.

[8]Arkhipov, B., Khoromsky, I., and Murashko, V., "Problems of designing EPSs with SPTs Working on Krypton-Xenon Mixture," *Proceedings of the 38th AIAA/ASME/SAE/ASEE Joint Propulsion Conference and Exhibit*, No. AIAA-2002-3682, 2002.

[9]Garner, C. E., Brophy, J. R., Polk, J. E., and Pless, L. C., "Cyclic Endurance Test of a SPT-100 Stationary Plasma Thruster," *In the Proceeding of the 30th AIAA/SAE/ASME/ASEE Joint Propulsion Conference and Exhibit*, 1994, AIAA-94-2856.

[10]Sankovic, J. M., Hamley, J. A., and Haag, T. W., "Performance evaluation of the Russian SPT-100 thruster at NASA LeRC," *Proceedings of the 23rd International Electric Propulsion Conference*, 1993, IEPC-93-094.

[11]Corey, R. L., Gascon, N., Delgado, J. J., Gaeta, G., Munir, S., and Lin, J., "Performance and Evolution of Stationary Plasma Thruster Electric Propulsion for Large Communications Satellites," *Proceedings of the 28th AIAA International Communications Satellite Systems Conference*, No. AIAA 2010-8688, 2010.

[12]Haag, T. W. and Curran, F. M., "Arcjet Starting Reliability: A Multistart Test on Hydrogen/Nitrogen Mixtures," Tech. rep., Lewis Research Center, 1987, NASA Technical Memorandum 89867.

[13]Brown, D. L., *Investigation of Low Discharge Voltage Hall Thruster Characteristics and Evaluation of Loss Mechanisms*, Ph.D. thesis, University of Michigan, 2009.

[14]Brown, S. C., *Basic Data of Plasma Physics*, American Institute of Physics Press, New York, 1994.

[15]Hutchinson, I., *Principles of Plasma Diagnostics*, Cambridge University Press, New York, 1994.

[16]Marrese, C., Gallimore, A. D., Haas, J., Foster, J., King, B., Kim, S. W., and Khartov, S., "An Investigation of Stationary Plasma Thruster Performance with Krypton Propellant," *In the Proceedings of the 31st AIAA/ASME/SAE/ASEE Joint Propulsion Conference and Exhibit*, No. AIAA 95-2932, 1995.

[17]Kim, V., "Main Physical Features and Processes Determining the Performance of Stationary Plasma Thrusters," *Journal of Propulsion and Power*, Vol. 14, No. 5, 1998, pp. 736–743.

[18]Gnizdor, R., Kozubsky, K., Koryakin, A., Maslennikov, N., Pridannikov, S., and Day, M., "SPT100 Life Test with Single Cathode up to Total Impulse Two Million Nsec," *Proceedings of the 36th AIAA/ASME/SAE/ASEE Joint Propulsion Conference and Exhibit*, No. AIAA-98-3790, 1998.

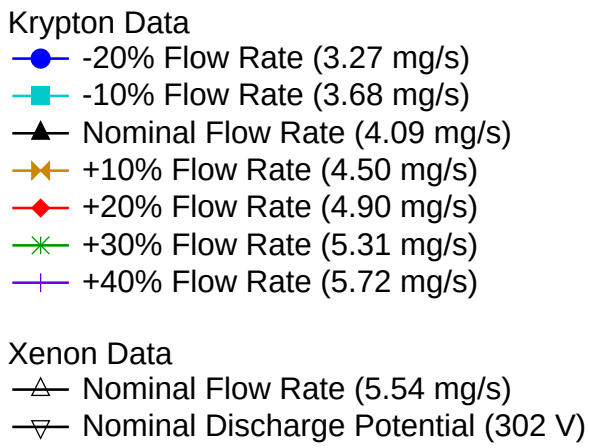

(a) Legend for performance plots.

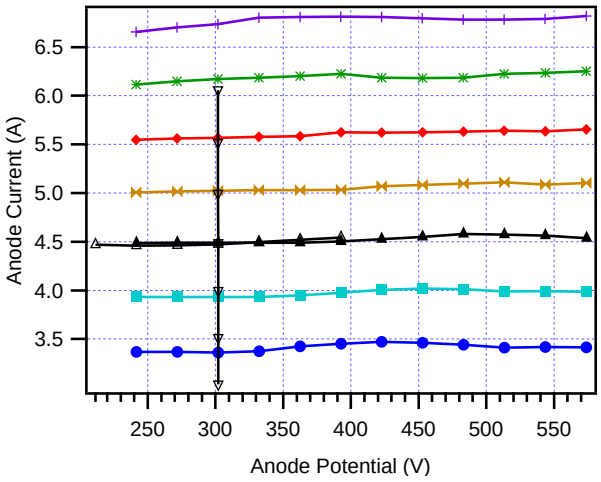

(b) Anode current vs. anode potential

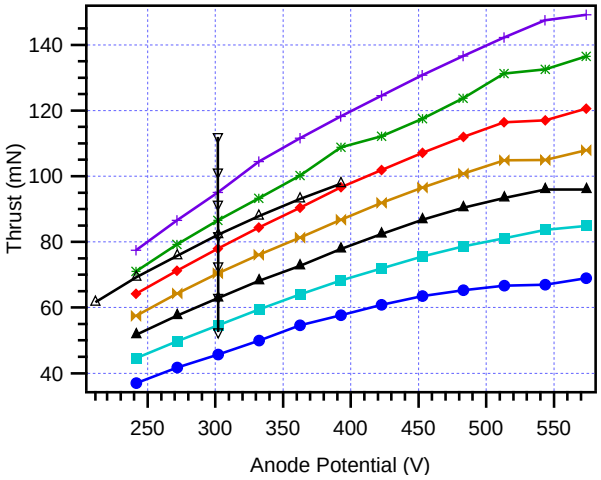

(c) Thrust vs. anode potential

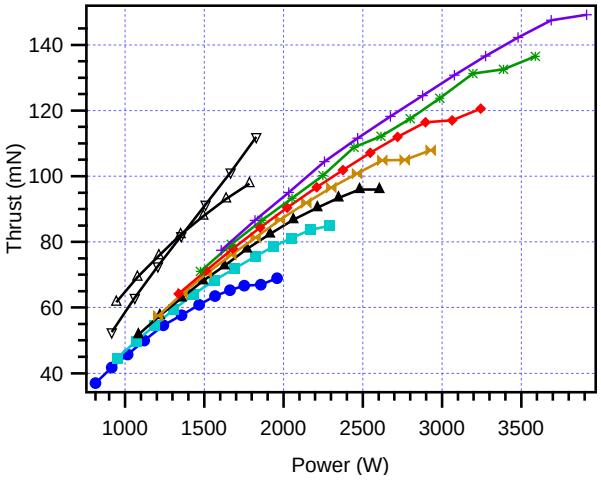

(d) Thrust vs. power

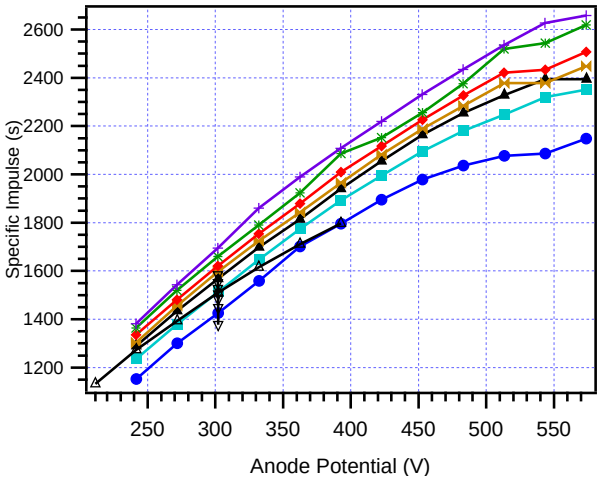

(e) Specific impulse vs. anode potential

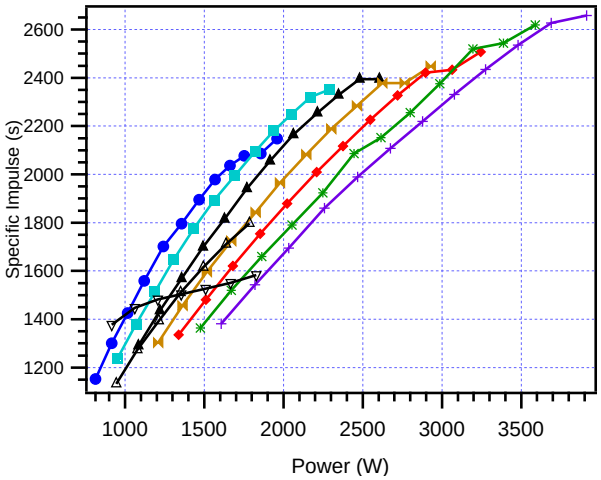

(f) Specific impulse vs. power

Figure 5. Thruster performance data.

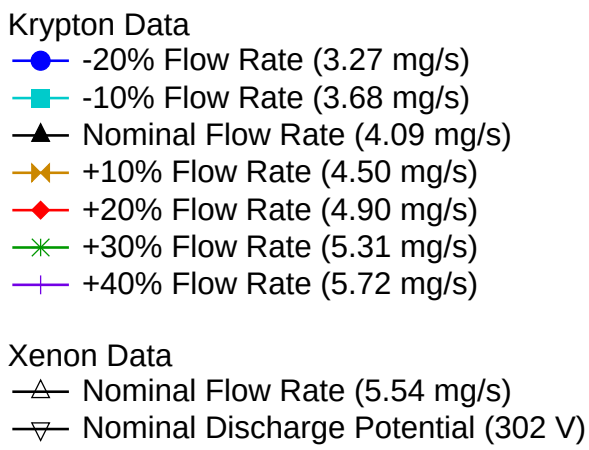

(a) Legend for performance plots.

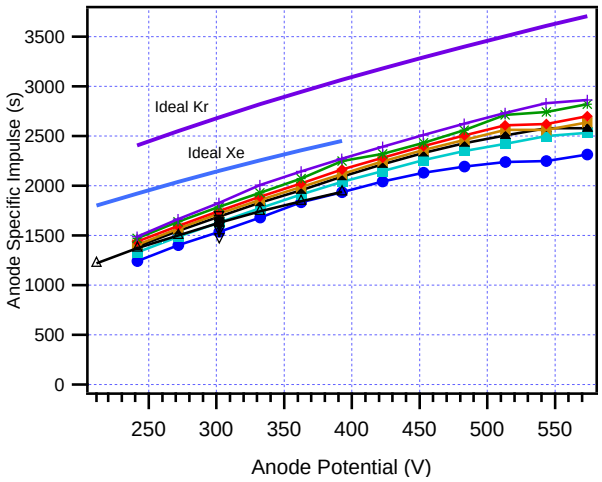

(b) Anode specific impulse vs. anode potential. Ideal values are shown for reference. (Note: Anode specific impulse calculation does not include cathode flow.)

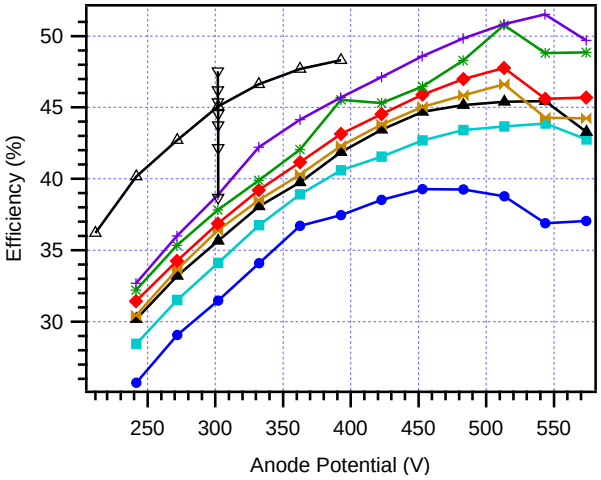

(c) Thrust efficiency vs. anode potential

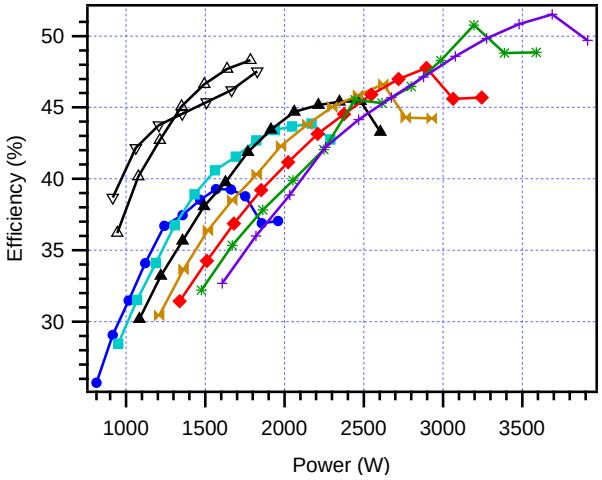

(d) Thrust efficiency vs. power

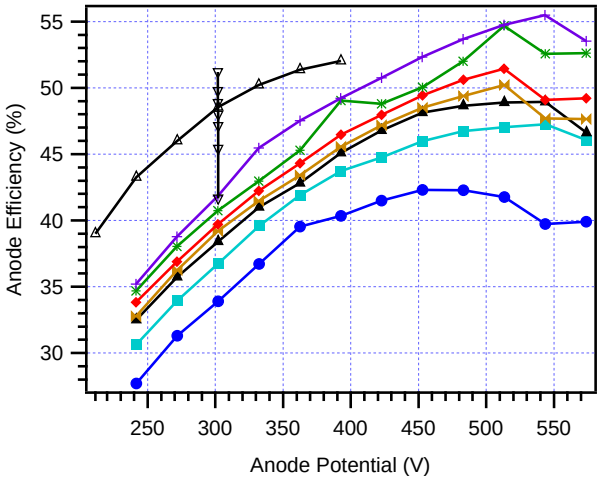

(e) Anode efficiency vs. anode potential (Note: Anode specific impulse calculation does not include cathode flow.)

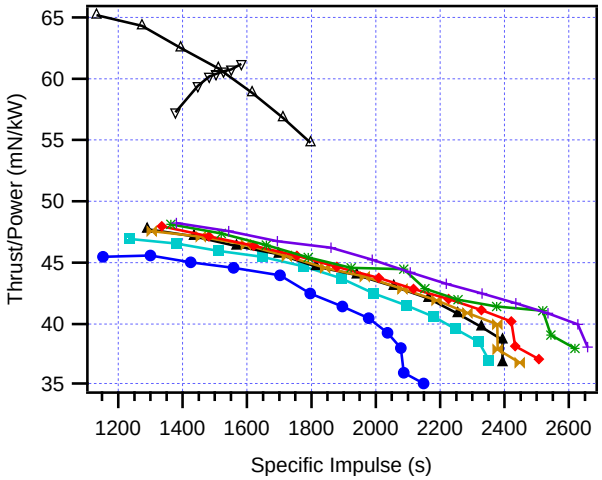

(f) Thrust to power ratio vs. specific impulse

Figure 6. Thruster performance data continued.

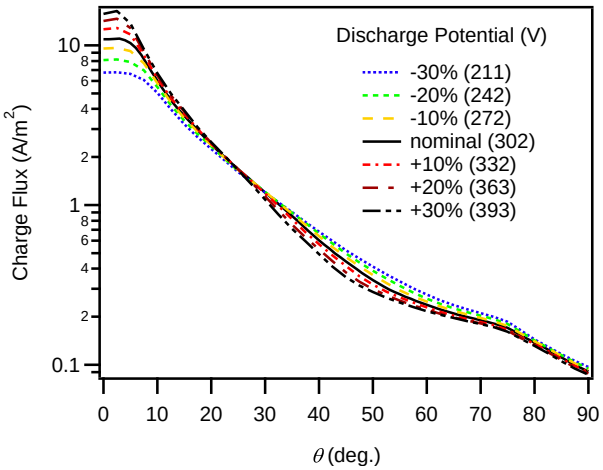

(a) Xe charge flux: discharge potential variations (nominal propellant flow rate: 5.54 mg/s, $r = 100$ cm)

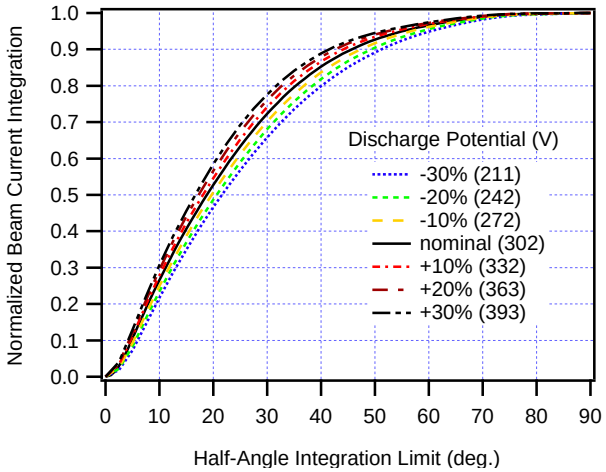

(b) Xe beam current integration: discharge potential variations (nominal propellant flow rate: 5.54 mg/s)

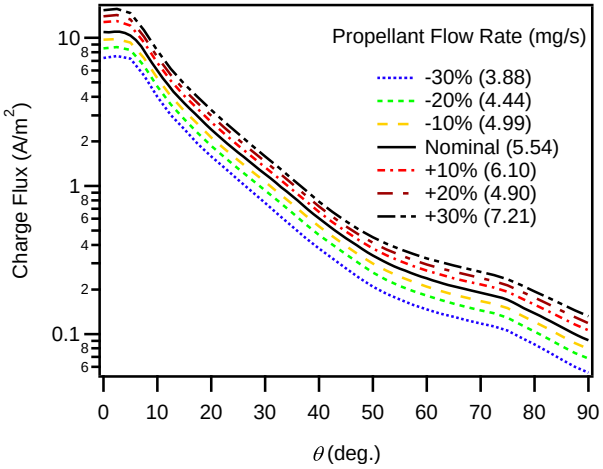

(c) Xe charge flux: propellant flow rate variations (nominal discharge potential: 302 V, $r = 100$ cm)

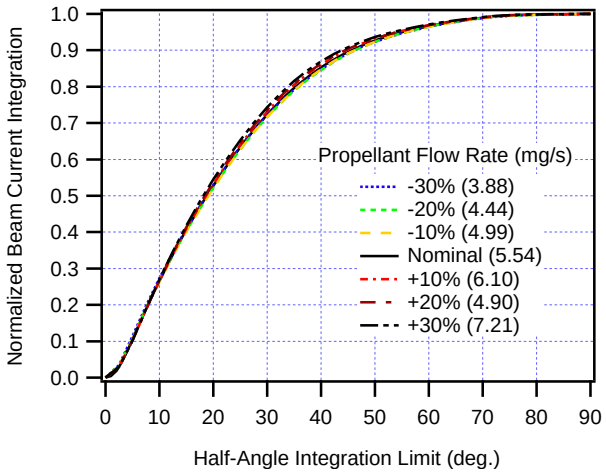

(d) Xe beam current integration: propellant flow rate variations (nominal discharge potential: 302 V)

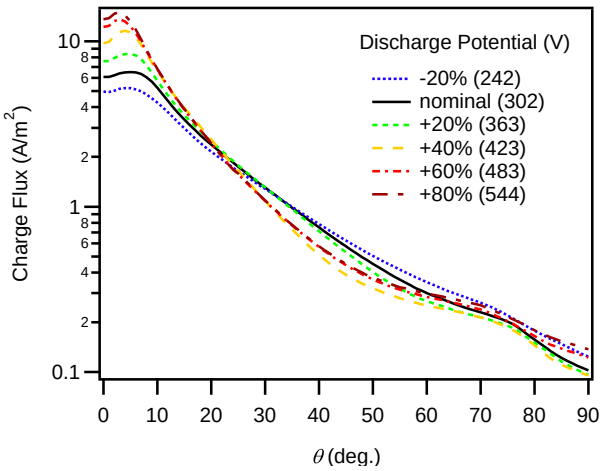

(e) Kr charge flux: discharge potential variations (nominal propellant flow rate: 4.09 mg/s, $r = 100$ cm)

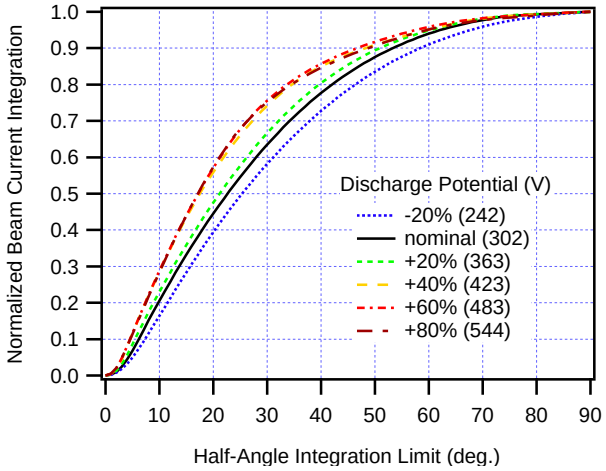

(f) Kr beam current integration: discharge potential variations (nominal propellant flow rate: 4.09 mg/s)

Figure 7. Faraday probe data

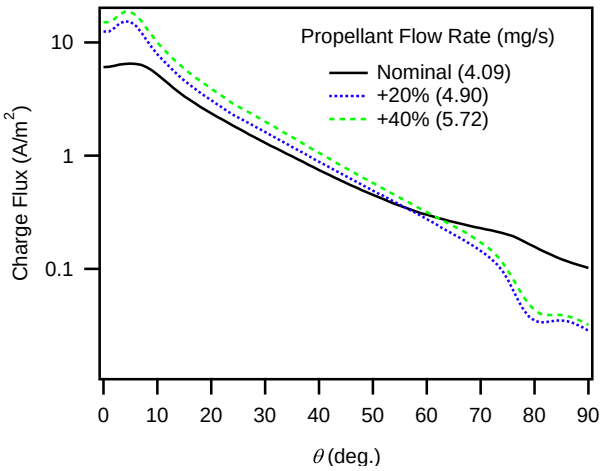

(a) Kr charge flux: propellant flow rate variations (nominal discharge potential: 302 V, $r = 100$ cm)

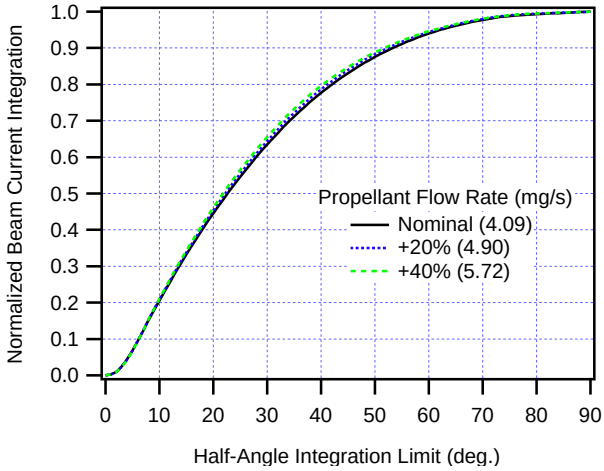

(b) Kr beam current integration: propellant flow rate variations (nominal discharge potential: 302 V)

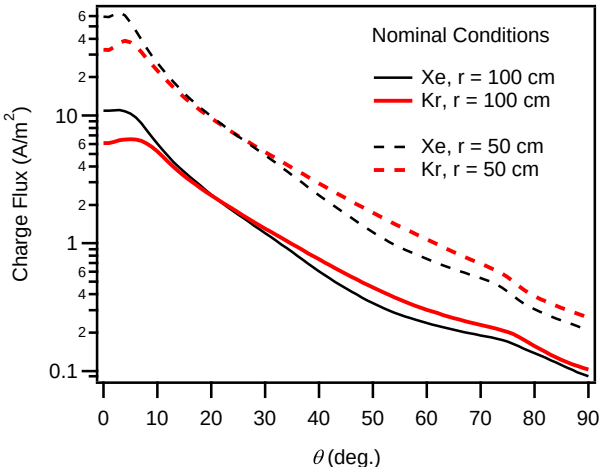

(c) Xe/Kr charge flux comparison: nominal conditions

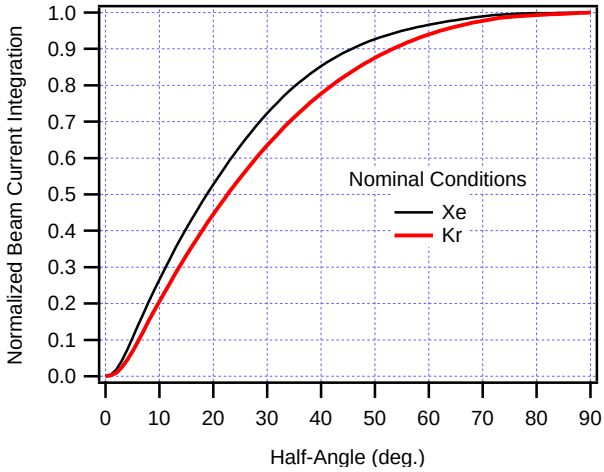

(d) Xe/Kr beam current integration comparison: nominal conditions

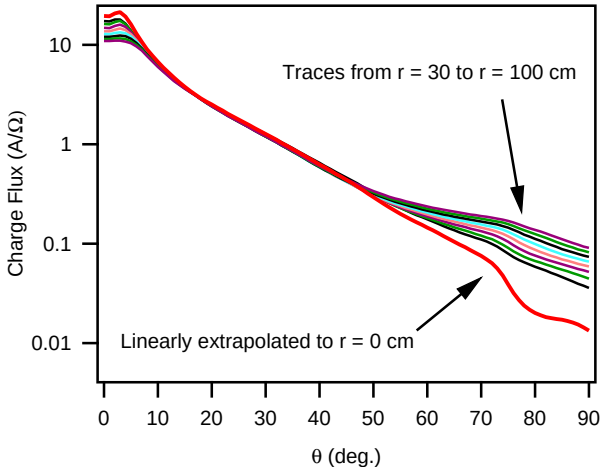

(e) Xe charge flux (current per solid angle) for different radii at nominal conditions. Charge flux at exit plane ($r = 0$) was linearly extrapolated as a function of r.

Figure 8. Faraday probe data continued

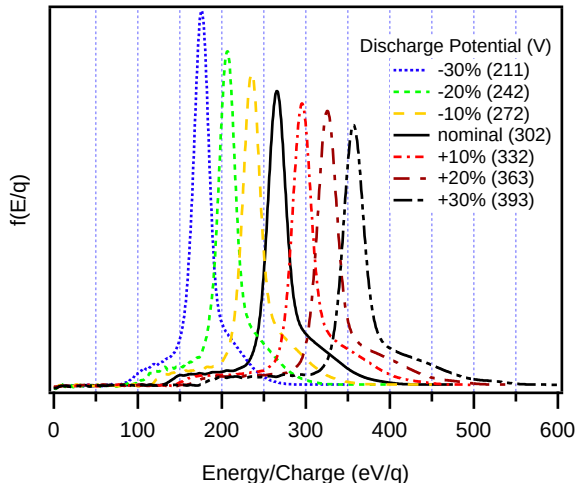

(a) Xe EDF: discharge potential variations (nominal propellant flow rate: 5.54 mg/s, $\theta = 0°$)

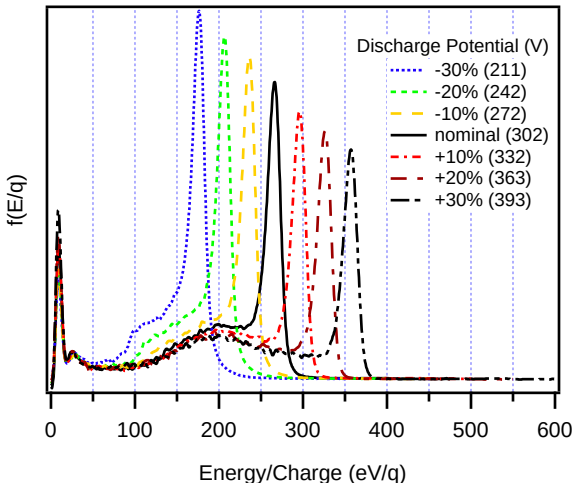

(b) Xe EDF: discharge potential variations (nominal propellant flow rate: 5.54 mg/s, $\theta = 45°$)

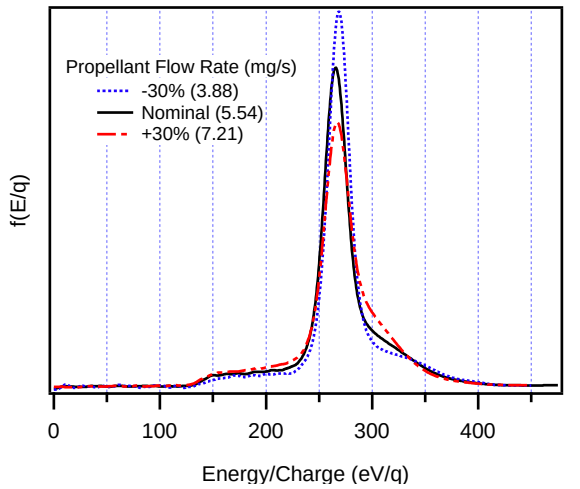

(c) Xe EDF: propellant flow rate variations (nominal discharge potential: 302 V, $\theta = 0°$)

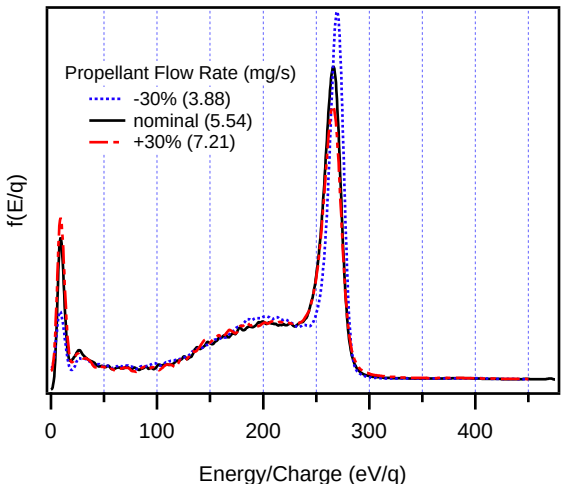

(d) Xe EDF: propellant flow rate variations (nominal discharge potential: 302 V, $\theta = 45°$)

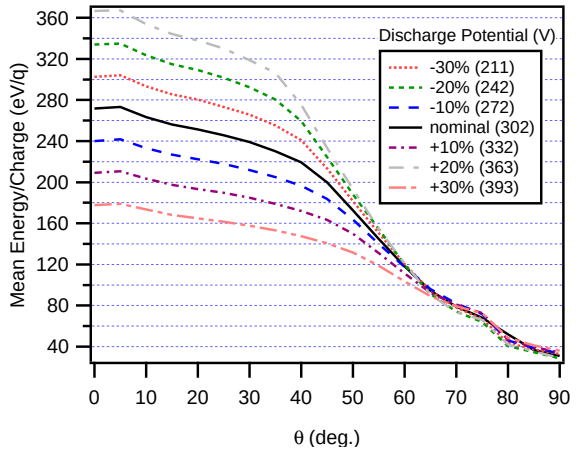

(e) Xe EDF mean: discharge potential variations (nominal propellant flow rate: 5.54 mg/s mean value)

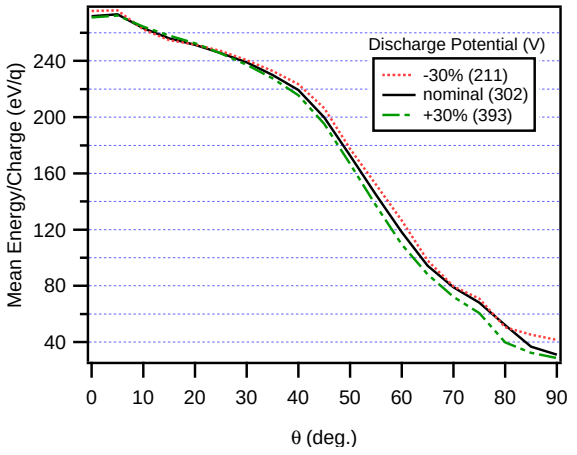

(f) Xe EDF mean: propellant flow rate variations (nominal discharge potential: 302 V)

Figure 9. Xe RPA data. Energy distribution functions are area normalized.

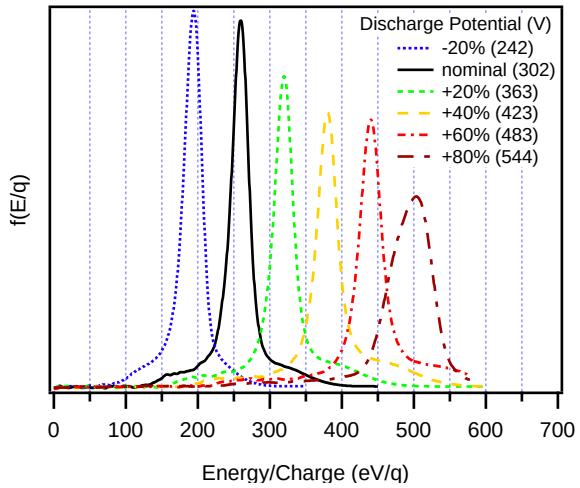

(a) Kr EDF: discharge potential variations (nominal propellant flow rate: 4.09 mg/s, $\theta = 0°$)

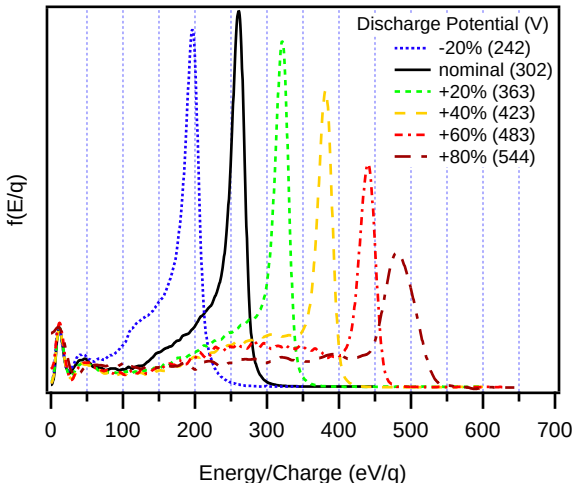

(b) Kr EDF: discharge potential variations (nominal propellant flow rate: 4.09 mg/s, $\theta = 45°$)

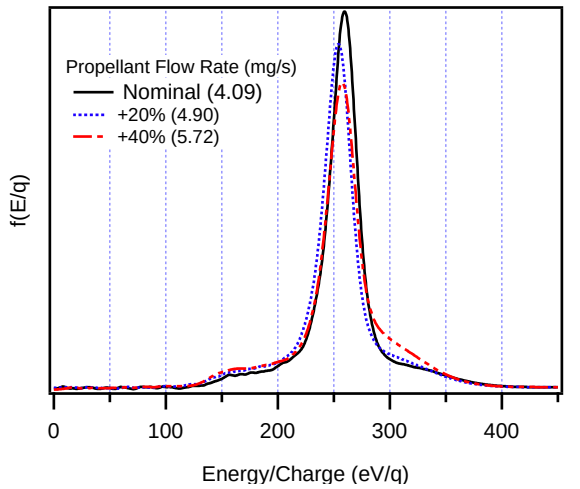

(c) Kr EDF: propellant flow rate variations (nominal discharge potential: 302 V, $\theta = 0°$)

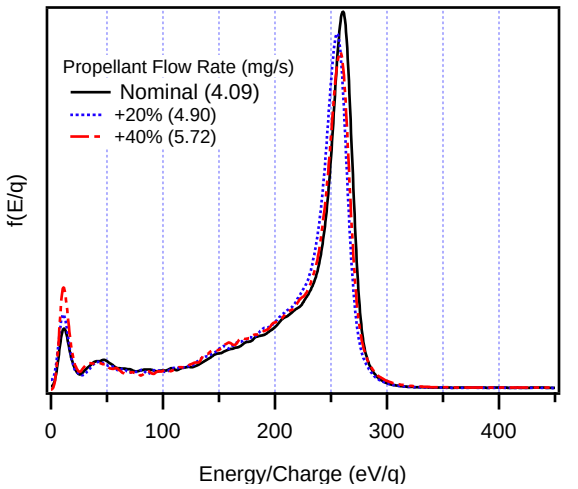

(d) Kr EDF: propellant flow rate variations (nominal discharge potential: 302 V, $\theta = 45°$)

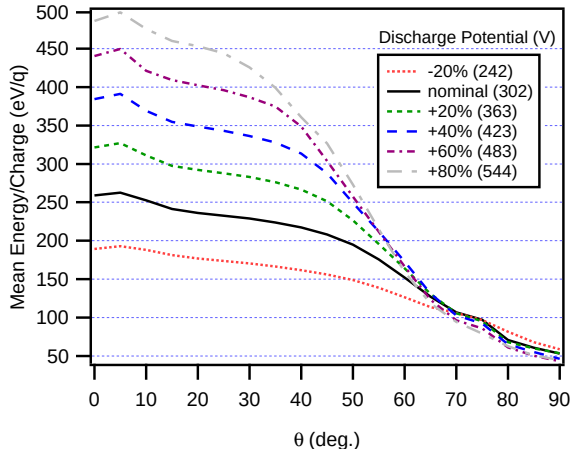

(e) Kr EDF mean: discharge potential variations (nominal propellant flow rate: 4.09 mg/s mean value)

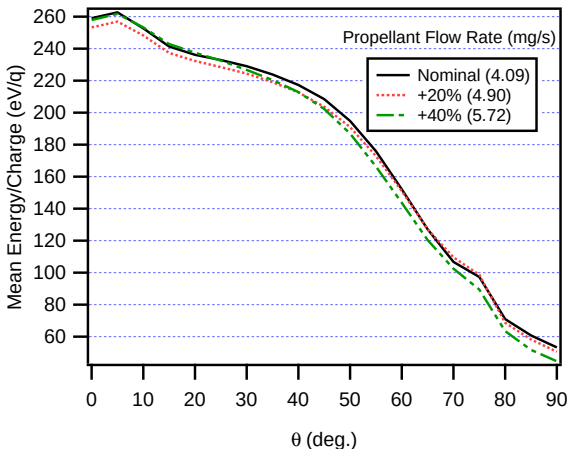

(f) Kr EDF mean: propellant flow rate variations (nominal discharge potential: 302 V)

Figure 10. Kr RPA data. Energy distribution functions are area normalized.

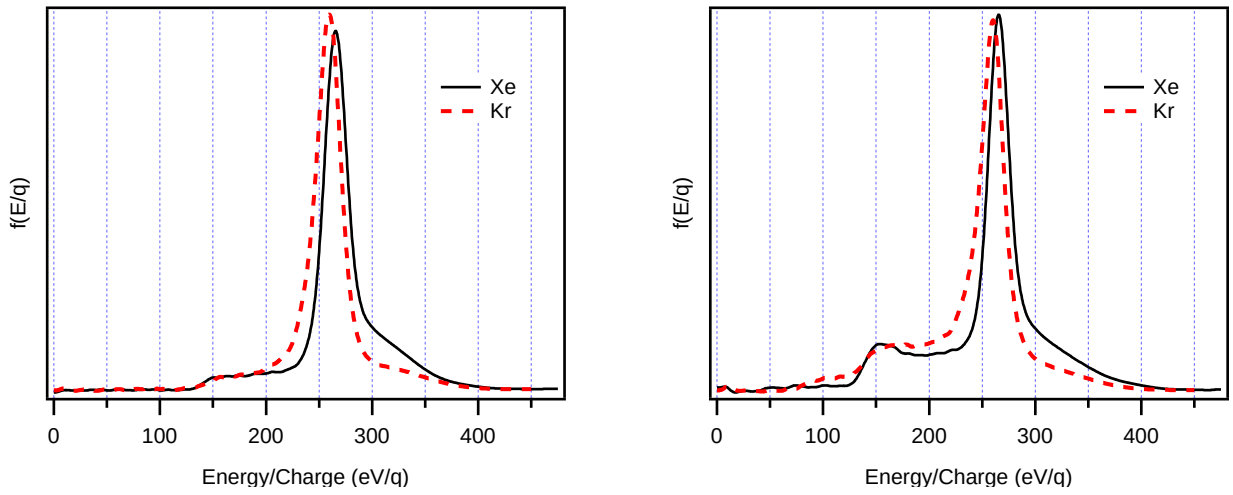

(a) $\theta = 0°$ (b) $\theta = 15°$

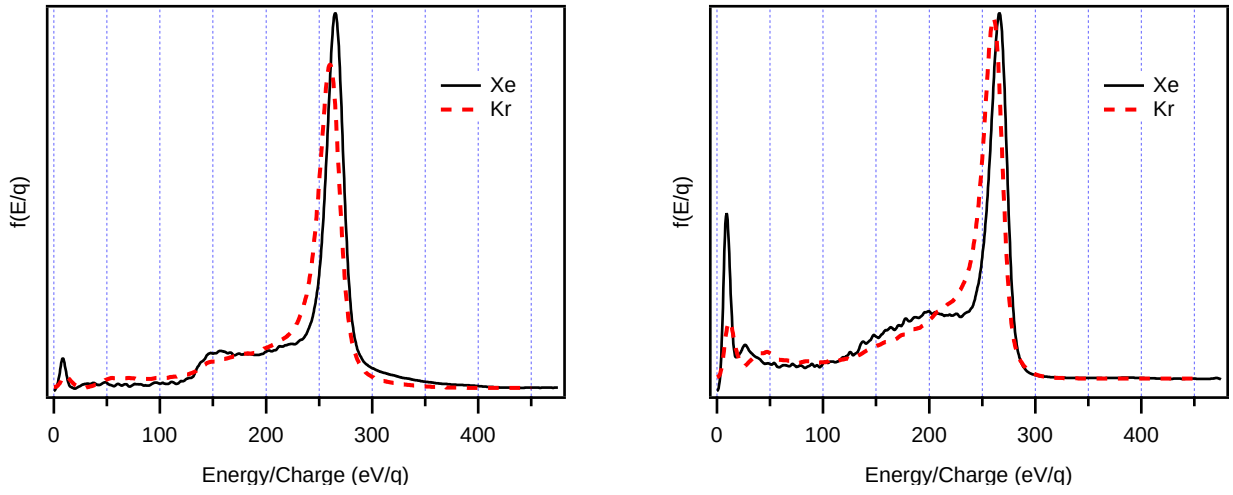

(c) $\theta = 30°$ (d) $\theta = 45°$

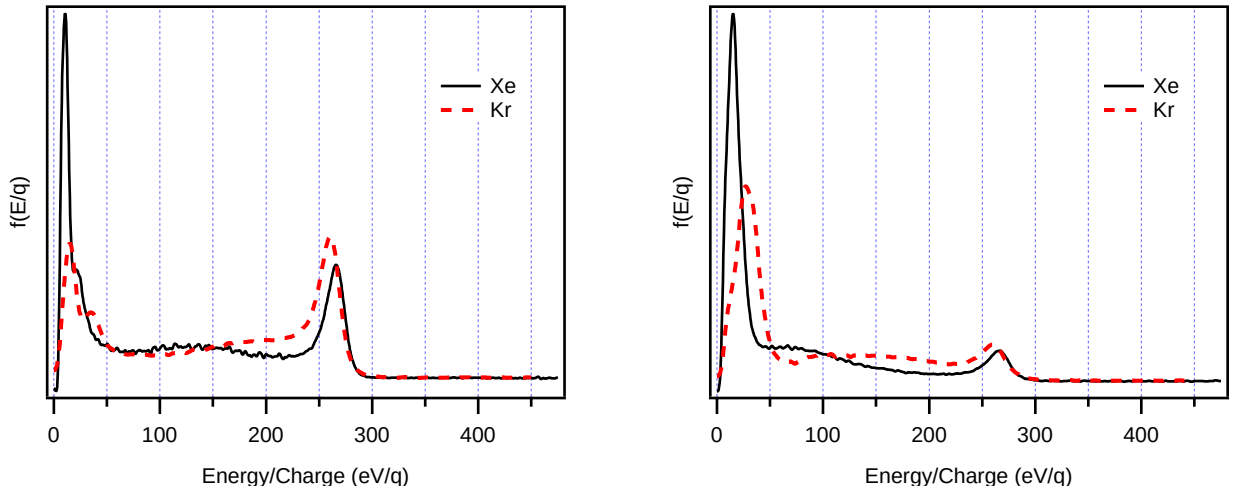

(e) $\theta = 60°$ (f) $\theta = 75°$

Figure 11. Xe/Kr EDF comparison for nominal operating condition at various angles. Energy distribution functions are area normalized.

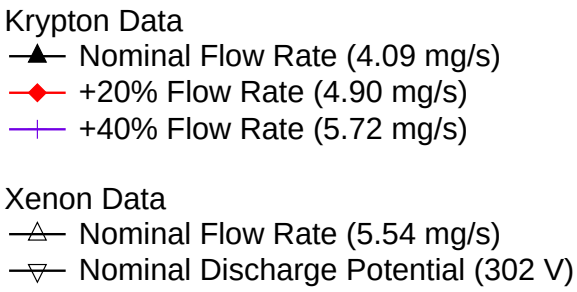

(a) Legend for probe-derived parameter plots.

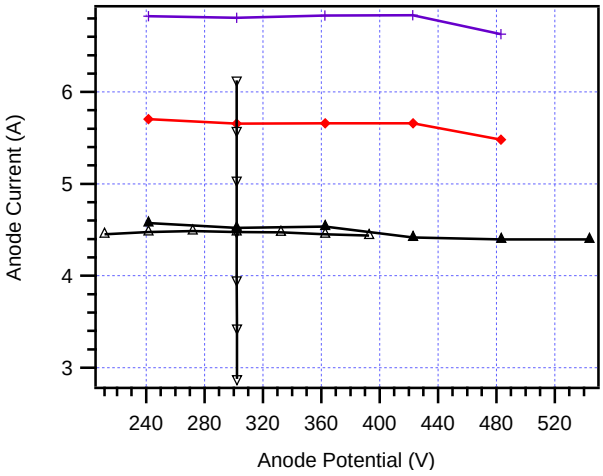

(b) Anode current vs. anode potential (Faraday probe measurements)

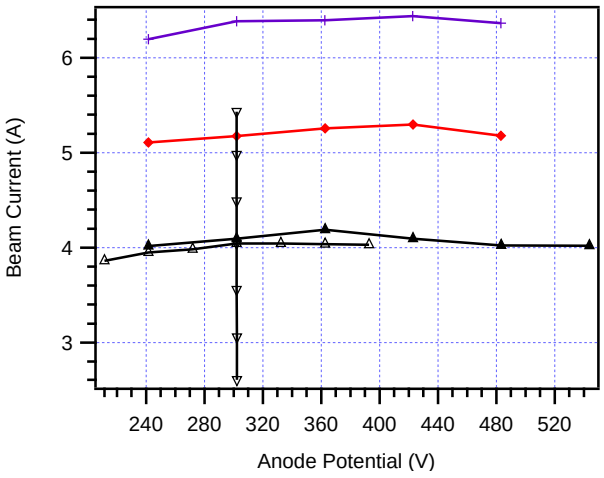

(c) Total integrated beam current vs. anode potential

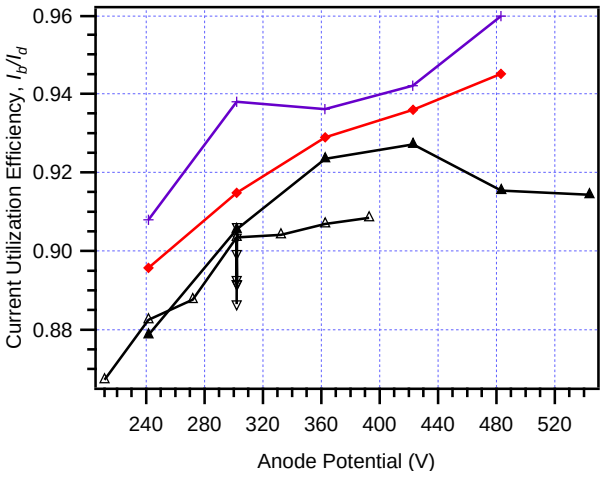

(d) Current utilization efficiency vs. anode potential

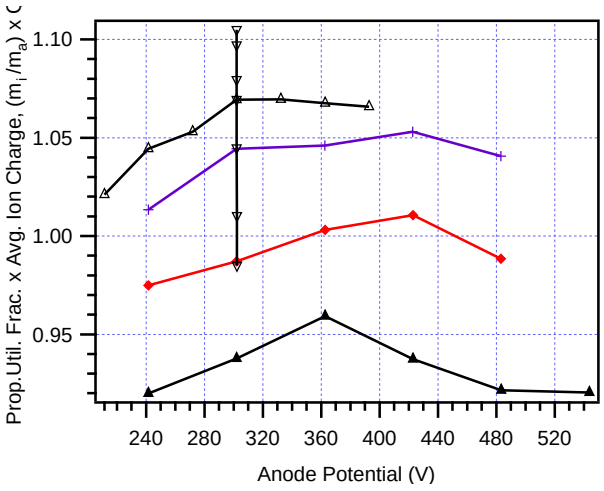

(e) Product of propellant utilization efficiency and average ion charge vs. anode potential

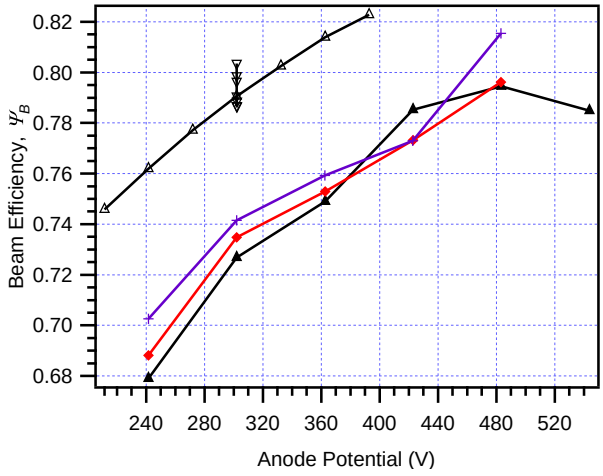

(f) Beam efficiency vs. anode potential

Figure 12. Probe derived performace characteristics.

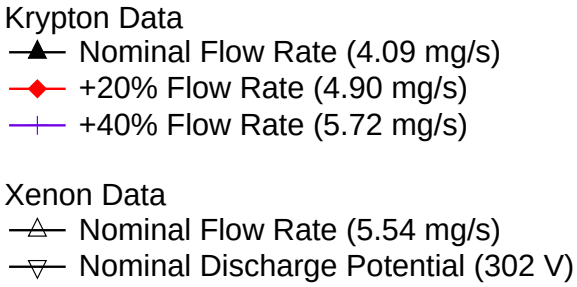

(a) Legend for probe-derived parameter plots.

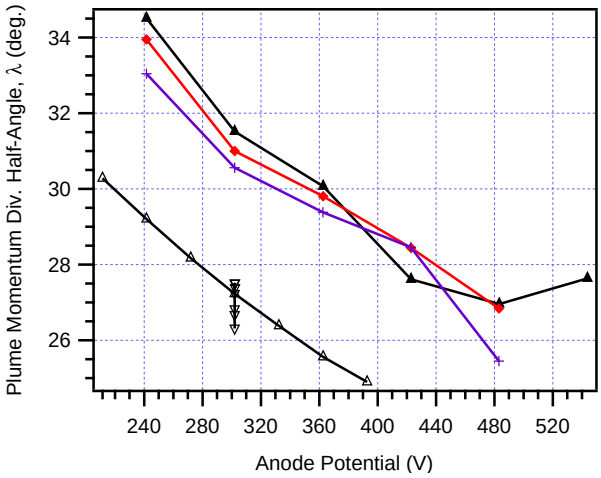

(b) Plume momentum divergence half-angle vs. anode potential

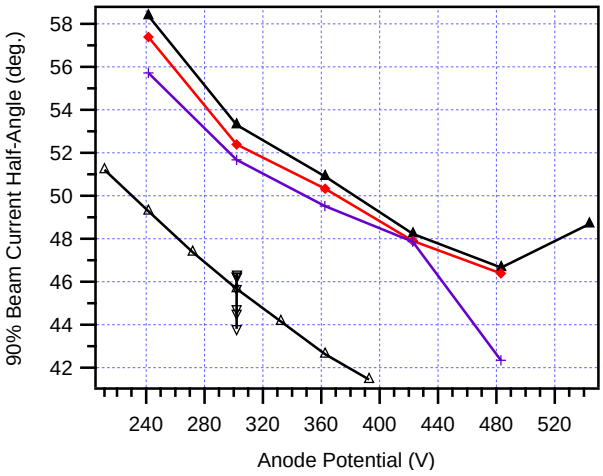

(c) 90% Beam current half-angle vs. anode potential

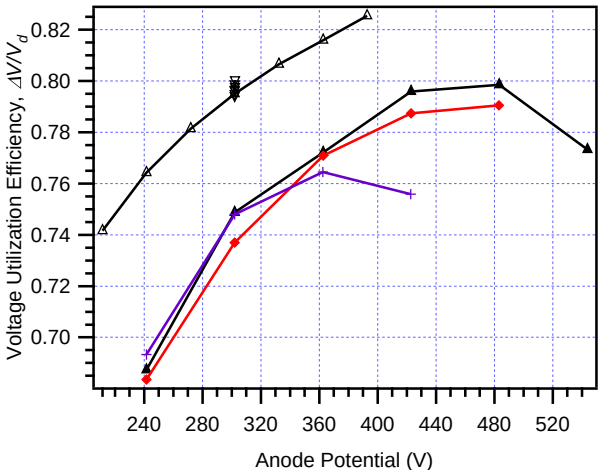

(d) Voltage utilization efficiency calculated using full energy distribution function range

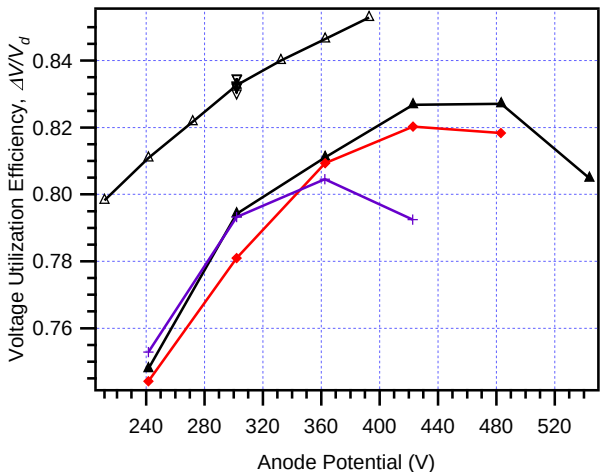

(e) Voltage utilization efficiency calculated using energy distribution function range above 100 eV/q

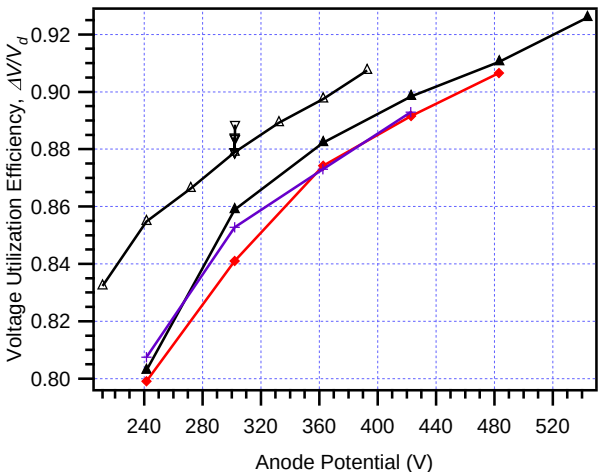

(f) Voltage utilization efficiency calculated using energy distribution function most probable value at $\theta = 0°$ deg.

Figure 13. Probe derived performance characteristics continued.